Int. J. Heat Mass Transfer. Vol. 35, No. 11, pp. 2969–2982, 1992
Printed in Great Britain

0017-9310/92 $5.00+0.00

A 1-D/2-D model and experimental results for a closed-loop thermosyphon with vertical heat transfer sections

M. A. BERNIER
Département de génie mécanique, Ecole Polytechnique de Montréal, Case postale 6079, succursale A, Montréal, Québec, Canada H3C 3A7

and

B. R. BALIGA
Department of Mechanical Engineering, McGill University, 817 Sherbrooke West, Montréal, Québec, Canada H3A 2K6

(*Received* 4 *June* 1991 *and in final form* 22 *November* 1991)

Abstract—In this paper, a new 1-D/2-D model is proposed for closed-loop thermosyphons with vertical heat transfer sections. This model improves the results of traditional 1-D models for cases where: (i) mixed-convection effects are important in the heated and cooled sections of the loop; and (ii) heat losses (or gains) from the insulated portions of the loop are significant. This is achieved by iteratively coupling local results of 2-D numerical simulations of mixed-convection flows, performed in the heated and cooled sections, and a 1-D analysis. The proposed 1-D/2-D model is validated by comparing its results with those of a complementary experimental study. The results include predictions and measurements of the average velocity in the loop, local wall temperatures in the heated section of the loop, and bulk temperatures of the fluid. The agreement between the model predictions and the experimental results is shown to be very good.

1. INTRODUCTION

CLOSED-LOOP thermosyphons are natural circulation loops in which fluid flow is induced by buoyancy forces. This paper is concerned with a numerical and experimental investigation of a closed-loop thermosyphon schematically illustrated in Fig. 1. It consists of two vertical straight pipes joined together by two circular 180° bends, each of mean radius R. All pipes are of circular cross-section with an internal radius r_i. The circulating fluid is heated by a constant and uniform heat flux, q ($= P_w/\pi DL_2$), in the heated section, and it is cooled in a cooling section maintained at a constant wall temperature, T_w. Elsewhere around the loop, the pipes are insulated. Of particular interest and importance in this study are the mixed-convection phenomena occurring in such a loop, as elaborated by Welander [1], in the heated and cooled sections.

Closed-loop thermosyphons have numerous engineering applications: examples include buoyancy driven natural circulation loops in small nuclear-powered systems for heating buildings [2]; internal combustion engines [3]; emergency cooling of nuclear reactor cores [4]; solar water heaters [5, 6]; and natural convection heat exchangers [7]. The main advantage provided by closed-loop thermosyphons is that they can transport heat from a source to a sink without a pump. For the proper design of all these engineering systems, the modelling of closed-loop thermosyphons is important. Excellent review articles on the modelling of closed-loop thermosyphons have been presented by Zvirin [4], Mertol and Greif [8], and Greif [9]. Therefore, only salient features of the relevant papers will now be described briefly.

So-called 1-D models have been used to predict the

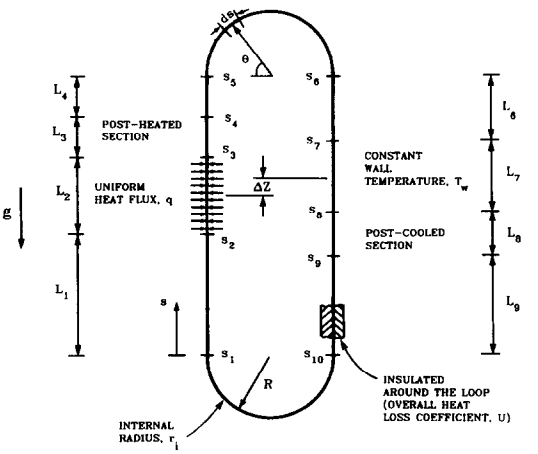

FIG. 1. Schematic illustration of the closed-loop thermosyphon used in the present study.

NOMENCLATURE

A cross-sectional area of the pipe
C_p specific heat of the fluid at constant pressure
D internal diameter of the pipe, $2r_i$
f Fanning friction factor, $\tau_w/(\rho V^2/2)$
Gr_m modified Grashof number, $D^3g\beta q/\nu V_{ref}k_f$
Gr_q Grashof number based on heat flux, $g\beta qD^4/\nu^2k_f$
g acceleration due to gravity
h heat transfer coefficient [W m^{-2} °C^{-1}]
i axial grid location
k_f thermal conductivity of the fluid
L total length of the closed-loop
L_1–L_9 various lengths of the closed-loop (Fig. 1)
$L1$ number of grid points in the axial direction
Nu Nusselt number, hD/k_f
p pressure
P^* non-dimensional pressure
P_w power input [W]
Pr Prandtl number, $\mu C_p/k_f$
q heat flux [W m^{-2}]
Q_x, Q_y, Q_z various heat losses in the loop
Re Reynolds number, VD/ν
Re_{ref} reference Reynolds number, $V_{ref}D/\nu$
R radius of the 180° bends (Fig. 1)
r radial coordinate
r_i internal radius of the pipe
s axial coordinate around the closed-loop
s_1–s_{10} given values of the axial coordinate
St_m modified Stanton number, $UD/\rho V_{ref}AC_p$
T area-weighted mean cross-sectional temperature
T_a ambient temperature
$T_{b,in}, T_{b,out}$ inlet, outlet bulk temperatures
T_m mean temperature in the closed-loop, $(T_2+T_3)/2$
T_w mean wall temperature in the cooled section
$T_{w,hs}$ local wall temperatures in the heated section
T_1–T_{10} nodal temperatures evaluated at s_1–s_{10}
u, v axial and radial velocity components
U overall heat loss coefficient [W m^{-1} °C^{-1}]
V average velocity
V_s average velocity in the heated section
V^* non-dimensional average velocity, V_s/V_{ref}
V_{ref} reference velocity, $(P_w\beta g\Delta Z/8\pi\mu C_pL)^{1/2}$
X parameter used in equation (8), $h2\pi r_i/\rho VAC_p$
z axial coordinate.

Greek symbols

β thermal volumetric expansion coefficient
Δs length of an elemental control volume
ΔZ height difference between the middle of the heated and cooled sections (Fig. 1)
ε length parameter, $(L_7/2)-(1/X)+[e^{-XL_7}/(1-e^{-XL_7})]L_7$
θ angle of the control volume in the thermosyphon (Fig. 1)
μ dynamic viscosity of the fluid
ξ parameter used in the z-momentum equation
ρ density of the fluid
τ_w shear stress at the wall
ϕ_∞ dimensionless ambient temperature, $(T_a-T_w)/(qD/k_f)$
Ω modified heat loss coefficient, $U/\rho VAC_p$.

Subscripts

cs refers to the cooled section
hs refers to the heated section.

velocity and temperature distributions in toroidal thermosyphons [10, 11] and in closed-loop thermosyphons with vertical heat transfer sections [12, 13]. In these 1-D models, velocities and temperatures are averaged over the cross-sectional area of the pipe, and the flow and heat transfer are assumed to be fully developed inside the whole loop. Such models, which are based on the assumption of fully developed conditions throughout the loop, will be referred to as *traditional* 1-D models in this paper. As shown by Lewis *et al.* [14] and Mertol *et al.* [15], the validity of traditional 1-D models becomes questionable for cases where buoyancy effects significantly influence the velocity and temperature profiles inside the loop.

In an attempt to improve the accuracy of traditional 1-D models, Durig and Shadday [16] used 2-D numerical simulations of mixed-convection flow to obtain estimates of the average friction factors and average heat transfer coefficients in the heated and cooled sections of closed-loop thermosyphons with vertical heat transfer sections. However, their 2-D numerical simulations were decoupled from the solution to the 1-D model. Such a decoupled 1-D/2-D approach is not very convenient. Furthermore, it could require numerous 2-D simulations, since the average velocity in the loop is not known *a priori*, and developing mixed-convection flows have to be modeled in the heated and cooled sections.

Lewis *et al.* [14] used local results of 2-D numerical simulations of mixed-convection flows to predict flow

rates in a thermosyphon loop comprised of two vertical tubes joined by upper and lower plenums. In the model of Lewis *et al.* [14], local values of the friction factor and of the mean cross-sectional temperature in the tubes are obtained numerically and then substituted into a general 1-D momentum equation where the only unknown left is ΔZ, the height difference between the middle of the heated section and the middle of the cooled section (Fig. 1). However, their numerical simulations were performed with the parabolic forms of the governing equations, thus limited to cases where mixed-convection effects do not induce a reversal of the flow in the tubes.

Another way to improve the velocity and temperature predictions is to numerically solve the complete 3-D governing equations. Lavine [17] has explored this avenue in a toroidal thermosyphon. Her results indicate that the computational cost (storage and CPU time) involved in such a calculation could be considerable.

Experiments have been performed to ascertain the validity of the afore-mentioned models. Creveling *et al.* [18], Damerell and Schoenhals [11], and Stern *et al.* [19] have studied experimentally the flow inside toroidal thermosyphons. Zvirin [4] and Vijayan and Date [20] have reported experiments performed on a small scale nuclear reactor operating under natural circulation. Hallinan and Viskanta [12] have conducted a series of experiments on the heat transfer from a vertical tube bundle in a natural circulation loop. The behavior of a rectangular closed-loop thermosyphon with vertical heat transfer passages, similar in shape to the one presented in this study, has been studied by Huang [21] and Huang and Zelaya [13]. The results of these experimental studies indicate that traditional 1-D models are accurate when conditions approach the fully developed state throughout the loop. However, when experimental conditions are such that local natural convection effects are strong in the heated and cooled sections, the velocity and temperature profiles are distorted from their fully developed forced convection shapes, and the traditional 1-D models become inaccurate.

In this study, a new approach, with accuracy, complexity, and computational costs in between those of traditional 1-D models and complete 3-D numerical simulations, is proposed to model closed-loop thermosyphons with vertical heat transfer sections. In this approach, the local results of 2-D numerical simulations of mixed-convection flows, performed in the heated and cooled sections of the thermosyphon, are coupled with a 1-D analysis, with a proper account of heat losses (or gains) from other sections of the loop.

The remainder of this paper is divided into three main sections: first, the governing equations and solution procedure of the proposed 1-D/2-D model are presented; then, the experimental apparatus is described; finally, the results of the experimental investigation are used to validate the proposed 1-D/2-D model.

2. PROPOSED 1-D/2-D MODEL

In this section, the assumptions used in the proposed 1-D/2-D model are presented first. Then the 1-D analysis used in the proposed model is reviewed. Following that, solutions of a *traditional* 1-D model are presented concisely, for the loop shown in Fig. 1. Next, the governing equations of the 2-D models of the heated and cooled sections are presented. Finally, a brief discussion of a coupled solution procedure used in the proposed 1-D/2-D model is given.

2.1. *Assumptions*

The assumptions used in the development of the proposed 1-D/2-D model of the closed-loop thermosyphon depicted in Fig. 1 are the following: (i) the fluid is Newtonian, and in single phase; (ii) the flow is steady and laminar; (iii) viscous heating is negligible; (iv) fluid flow and heat transfer are assumed to be 2-D and axisymmetric in the extended heated section (which includes the heated and post-heated sections) and the extended cooled section (which includes the cooled and post-cooled sections); (v) at the entrance to the heated and cooled sections, the flow is fully developed (Poiseuille parabola) and the temperature is uniform; (vi) the fluid properties are constant, and evaluated at the mean loop temperature T_m ($=[T_2+T_3]/2$), with the use of the Boussinesq approximation in the treatment of the density; (vii) curvature effects and associated form losses are negligible; and (viii) heat conduction in the pipe, and axial conduction in the fluid outside the extended heated and cooled sections, are negligible.

2.2. *One-dimensional analysis*

Application of the principle of conservation of momentum to an elemental control volume, in the context of 1-D flow throughout the loop, gives a balance between the pressure force, the shear force on the pipe wall, and the gravitational force [10, 22]. Integrating this balance along path 's' around the loop yields (Fig. 1)

$$V^2 \oint f(s)\,\mathrm{d}s = r_i g\beta \oint T(s)\cos\theta\,\mathrm{d}s \qquad (1)$$

where V is the average velocity inside the loop, f is the Fanning friction factor, r_i is the internal radius of the pipe, g is the gravitational acceleration, θ is the angle of the elemental control volume with respect to the horizontal (Fig. 1), $T(s)$ is the fluid temperature in the cross-section of interest, and β is the thermal volumetric expansion coefficient of the fluid.

In order to solve equation (1), values of $f(s)$ and $T(s)$ need to be evaluated at all locations around the loop. In the proposed 1-D/2-D model, $f(s)$ and $T(s)$ values in the extended heated and cooled sections are obtained from the results of detailed 2-D numerical simulations (discussed in Section 2.4). In sections other than the extended heated and cooled sections,

$f(s)$ is set equal to $16/Re$, and $T(s)$ is determined by deriving and solving a 1-D energy equation with a proper account of the heat losses (or gains); details are available in ref. [22]. With these considerations, and with reference to Fig. 1, the 1-D momentum equation (equation (1)) takes the following form

$$V^2\left[\frac{16}{Re}\int_{s_0}^{s_2} ds+\int_{s_2}^{s_4} f_{hs}(s)\,ds + \frac{16}{Re}\int_{s_4}^{s_7} ds+\int_{s_7}^{s_9} f_{cs}(s)\,ds\right] = r_i g\beta\left[\int_{s_0}^{s_2} T(s)\cos\theta\,ds+\int_{s_2}^{s_4} T_{hs}(s)\,ds + \int_{s_4}^{s_7} T(s)\cos\theta\,ds-\int_{s_7}^{s_9} T_{cs}(s)\,ds\right]. \quad (2)$$

In regions outside the extended heated and cooled sections, heat losses (or gains) are accounted for through an overall heat loss coefficient, U (in W m^{-1} °C^{-1}): U is assumed constant, as the insulation level is the same everywhere and it constitutes the dominant thermal resistance. Using the section from s_4 and s_5 as an example, the corresponding temperature distribution can be expressed as

$$T(s) = (T_4 - T_a)\,e^{-\Omega(s-s_4)} + T_a \quad (s_4 < s < s_5) \quad (3)$$

where $\Omega = U/\rho VAC_p$, C_p is the specific heat of the fluid at constant pressure, ρ is the density of the fluid, and A is the cross-sectional area of the pipe.

2.3. *Traditional 1-D model*

In traditional 1-D models, the flow is assumed to be fully developed throughout the loop, so that $f(s) = 16/Re$ everywhere. The temperature distribution around the loop, $T(s)$, is determined by deriving and solving the 1-D energy equation, with adiabatic conditions assumed in sections other than the heated and cooled sections. In the heated and cooled sections, two sets of thermal boundary conditions, which are identified as *case* (1) and *case* (2) in this paper, will be examined. For *case* (1), the thermal boundary conditions are: (i) constant heat flux in the heated section, and (ii) constant cooling flux in the cooled section. For *case* (2), the thermal boundary conditions are: (i) constant heat flux in the heated section; and (ii) constant wall temperature in the cooling section with a thermally fully developed condition ($Nu = 3.66$).

For *case* (1), with respect to the nomenclature presented in Fig. 1, $T(s)$ is given by the following equations:

for $s_2 \leqslant s \leqslant s_3$

$$T(s) = T_2 + \frac{(s-s_2)}{\rho VAC_p}\frac{P_w}{L_2} \quad (4)$$

for $s_3 < s < s_7$

$$T(s) = T_3 \quad (5)$$

for $s_7 \leqslant s \leqslant s_8$

$$T(s) = T_7 - \frac{(s-s_7)}{\rho VAC_p}\frac{P_w}{L_7} \quad (6)$$

and for $s_8 < s < s_2$

$$T(s) = T_8 \quad (7)$$

where P_w is the power input, V is the average fluid velocity in the sections of interest, and L_2 and L_7 are the lengths of the heated and cooled sections, respectively. Temperatures T_1–T_{10}, which will be referred to as nodal temperatures, are evaluated at their corresponding axial locations, s_1–s_{10}: $T_4 = T_5 = T_6 = T_7 = T_3$, and $T_9 = T_{10} = T_1 = T_2 = T_8$.

For *case* (2), the equations in the heated and adiabatic sections are the same as those for *case* (1). In the cooled section ($s_7 \leqslant s \leqslant s_8$)

$$T(s) = (T_7 - T_w)\,e^{-X(s-s_7)} + T_w \quad (8)$$

where

$$X = \frac{h2\pi r_i}{\rho VAC_p} = \frac{\pi k_f Nu}{\rho VAC_p},$$

with $Nu = 3.66$, h is the heat transfer coefficient in the cooled section, k_f is the thermal conductivity of the fluid, and T_w is the constant wall temperature in the cooled section.

Equation (1) can now be solved using the temperature distributions given in equations (5)–(8). Details of the solution can be found in the work of Bernier [22]. The end result, in its general form, which includes *cases* (1) and (2), is

$$V = \left[\frac{P_w\beta g}{8\pi\mu C_p L}(\Delta Z+\varepsilon)\right]^{1/2} \quad (9)$$

where

$$\varepsilon = 0 \quad \text{for } case\ (1)$$

$$\varepsilon = \frac{L_7}{2} - \frac{1}{X} + \frac{e^{-XL_7}}{1-e^{-XL_7}}L_7 \quad \text{for } case\ (2)$$

and ΔZ is the height difference between the middle of the cooled section and the middle of the heated section, as shown in Fig. 1. For *case* (2), ε can be regarded as a correction factor to account for the exponential variation of the fluid temperature in the cooled section.

2.4. *Two-dimensional models in the extended heated and cooled sections*

The calculation domain as well as the boundary conditions for the extended heated and cooled sections are presented in Figs. 2(a) and (b), respectively. As shown in both figures, the calculation domains are not restricted only to the heated or cooled sections, but include sections downstream of the heated and cooled sections. These 'post'-sections are included in the calculation domain because both the velocity and the temperature profiles remain distorted from their

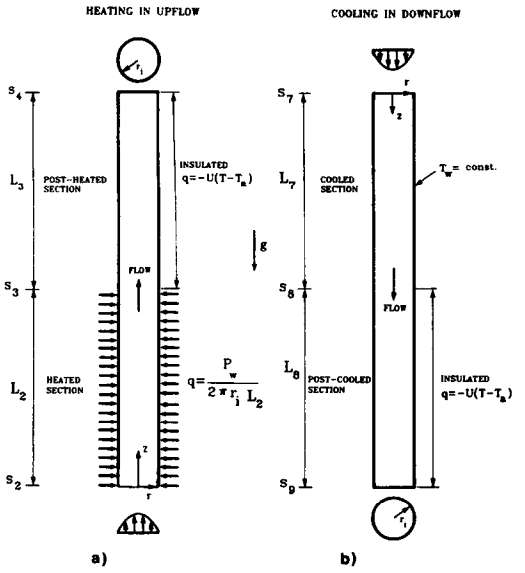

FIG. 2. Calculation domain and boundary conditions used in the two-dimensional numerical simulations of the proposed model: (a) the extended heated section; and (b) the extended cooled section.

fully developed shapes for some distance after the heated or cooled sections.

In the extended heated and cooled sections, fluid flow and heat transfer are governed by the Navier–Stokes equations, the continuity equation, and the energy equation, all in cylindrical coordinates. As discussed in the work of Bernier [22], elliptic forms of these equations are required when flow reversals occur and/or axial conduction in the fluid is significant: otherwise, parabolic forms of the governing equations are adequate, and more economical to use. In this paper, however, only the elliptic forms of the governing equations will be presented.

With the assumptions given earlier, the elliptic forms of the governing equations are

Continuity equation

$$\frac{1}{r}\frac{\partial(rv)}{\partial r}+\frac{\partial u}{\partial z}=0 \tag{10}$$

r-momentum equation

$$\rho\left[v\frac{\partial v}{\partial r}+u\frac{\partial v}{\partial z}\right]=-\frac{\partial p}{\partial r}+\frac{1}{r}\frac{\partial}{\partial r}\left[r\mu\frac{\partial v}{\partial r}\right]-\frac{\mu v}{r^2}+\frac{\partial}{\partial z}\left[\mu\frac{\partial v}{\partial z}\right] \tag{11}$$

z-momentum equation

$$\rho\left[v\frac{\partial u}{\partial r}+u\frac{\partial u}{\partial z}\right]=+\xi\rho g-\xi\dot{\beta}\rho g(T-T_m)-\frac{\partial p}{\partial z}+\frac{1}{r}\frac{\partial}{\partial r}\left[r\mu\frac{\partial u}{\partial r}\right]+\frac{\partial}{\partial z}\left[\mu\frac{\partial u}{\partial z}\right] \tag{12}$$

where $\xi = 1$ for the cooling in downflow case, and $\xi = -1$ for the heating in upflow case.

Energy equation

$$\rho C_p\left[v\frac{\partial T}{\partial r}+u\frac{\partial T}{\partial z}\right]=\frac{1}{r}\frac{\partial}{\partial r}\left[rk_f\frac{\partial T}{\partial r}\right]+\frac{\partial}{\partial r}\left[k_f\frac{\partial T}{\partial z}\right] \tag{13}$$

where u and v are the axial and radial velocities, respectively. Equations (10)–(13) are presented in a general form allowing for variable μ and k_f. However, in the momentum equations, terms such as $[(\partial\mu/\partial z)(\partial u/\partial r)]$, which are usually present when μ is not assumed constant, have been dropped: over the range of parameters investigated in this work [22], they were found to have no perceptible influence on the results.

In addition to the governing equations, boundary conditions are needed to complete the mathematical model. With reference to Figs. 1 and 2, these boundary conditions are

Inlet boundary conditions

For heating in upflow	For cooling in downflow
$s = s_2$	$s = s_7$
$z = 0$	$z = 0$
$u = 2V[1-(r/r_i)^2]$	$u = 2V[1-(r/r_i)^2]$
$T = T_2$	$T = T_7$

(14)

Boundary conditions in the heated and cooled sections

	For heating in upflow	For cooling in downflow
	$s_2 < s \leqslant s_3$	$s_7 < s \leqslant s_8$
	$0 < z \leqslant L_2$	$0 < z \leqslant L_7$
at $r = r_i$	$k_f\frac{\partial T}{\partial r} = q = \frac{P_w}{2\pi r_i L_2}$, $u = 0$, $v = 0$	$T = T_w$, $u = 0$, $v = 0$
at $r = 0$	$\frac{\partial T}{\partial r} = 0$, $\frac{\partial u}{\partial r} = 0$, $\frac{\partial v}{\partial r} = 0$	$\frac{\partial T}{\partial r} = 0$, $\frac{\partial u}{\partial r} = 0$, $\frac{\partial v}{\partial r} = 0$

(15)

Boundary conditions in the post-heated and post-cooled sections

For heating in upflow	For cooling in downflow
$s_3 < s \leqslant s_4$	$s_8 < s \leqslant s_9$
$L_2 < z \leqslant L_2 + L_3$	$L_7 < z \leqslant L_7 + L_8$

$$\text{at } r = r_i \quad \begin{cases} (2\pi r_i)k_f \dfrac{\partial T}{\partial r} = -U(T - T_a) \\ u = 0, \quad v = 0 \end{cases}$$

$$\text{at } r = 0 \quad \begin{cases} \dfrac{\partial T}{\partial r} = 0 \\ \dfrac{\partial u}{\partial r} = 0, \quad \dfrac{\partial v}{\partial r} = 0 \end{cases} \tag{16}$$

Outlet boundary conditions

For heating in upflow	For cooling in downflow
$s = s_4$	$s = s_9$
$z = L_2 + L_3$	$z = L_7 + L_8$

$$\frac{\partial u}{\partial z} = 0, \quad \frac{\partial v}{\partial z} = 0$$

$$\frac{\partial T}{\partial z} = 0. \tag{17}$$

In equation (16), U is an overall heat loss coefficient (in W m^{-1} °C^{-1}) and T_a is the ambient temperature.

2.5. *Coupled solution of the proposed 1-D/2-D model*

The values of $f(s)$ and $T(s)$ in the extended heated and cooled sections are determined numerically, and, therefore, they are discrete values prevailing over certain finite distances, Δs. Thus, the integrals related to the extended heated and cooled sections in equation (2) can be replaced by summations. Furthermore, the remaining integrals in equation (2), pertaining to regions other than the heated and cooled sections, can be solved using the temperature distributions given by equations similar to equation (3). With these considerations, the final form of the 1-D momentum equation of the proposed 1-D/2-D model is

$$V^2\left[\frac{16}{Re}(L_1 + L_4 + L_6 + L_9 + 2\pi R) + \sum_{i=1}^{i=L1} f_{hs,i}\Delta s_i + \sum_{i=1}^{i=L1} f_{cs,i}\Delta s_i\right]$$

$$= r_i g\beta\left[-\frac{(T_9 - T_a)}{\Omega}(1 - e^{-\Omega L_9}) - T_a L_9 + \frac{(T_1 - T_a)}{\Omega}(1 - e^{\Omega L_1}) + T_a L_1 + \sum_{i=1}^{i=L1} T_{hs,i}\Delta s_i + \frac{(T_4 - T_a)}{\Omega}(1 - e^{-\Omega L_4}) + T_a L_4 - \frac{(T_6 - T_a)}{\Omega}(1 - e^{-\Omega L_6}) - T_a L_6 - \sum_{i=1}^{i=L1} T_{cs,i}\Delta s_i + \frac{\Omega R^2(e^{\pi R\Omega} + 1)}{(\Omega^2 R^2 + 1)}(T_5 - T_{10})\right] \tag{18}$$

where the subscript 'i' refers to a particular grid location and $L1$ represents the total number of grid points in the axial direction, in each of the extended heat transfer sections. The Fanning friction factors, $f_{cs,i}$ and $f_{hs,i}$, and the mean cross-sectional temperatures, $T_{hs,i}$ and $T_{cs,i}$, are obtained by using suitable numerical approximations of

$$f_{hs}(s) \text{ or } f_{cs}(s) = \frac{\mu \left.\dfrac{\partial u}{\partial r}\right|_{r=r_i}}{\rho V^2/2} \tag{19}$$

$$T_{hs}(s) \text{ or } T_{cs}(s) = \frac{\int_A T(r, s)\, dA}{A}. \tag{20}$$

Equation (18) can be further expanded to include form losses in the loop, by adding an equivalent length of pipe, L_{eq}, to the first term on the left-hand side of the equation ($\ldots L_9 + 2\pi R + L_{eq}$). In addition, modifications to account for different radii in the various sections of the loop can be incorporated. Details are available in the work of Bernier [22].

In this work, the 2-D numerical simulations of mixed-convection flows in the extended heated and cooled sections were carried out using the well-established finite-volume method of Patankar [23]. The SIMPLEC procedure of Van Doormaal and Raithby [24] was used to solve the discretized equations produced by this finite-volume method. The solution of equation (18) requires inputs from 2-D numerical simulations which themselves depend on V. Therefore, equation (18) and the 2-D numerical simulations in the extended heated and cooled sections have to be carefully decoupled and solved iteratively to obtain V and the temperature distribution around the loop; details are given in ref. [22].

3. EXPERIMENTAL APPARATUS

3.1. *Overall design*

A closed-loop thermosyphon with vertical heat transfer passages was specially designed and constructed for the present investigation. It is presented schematically in Fig. 3. It consists of two sets of vertical Plexiglas pipe sections joined together by two circular 180° bends, which provide a smooth tran-

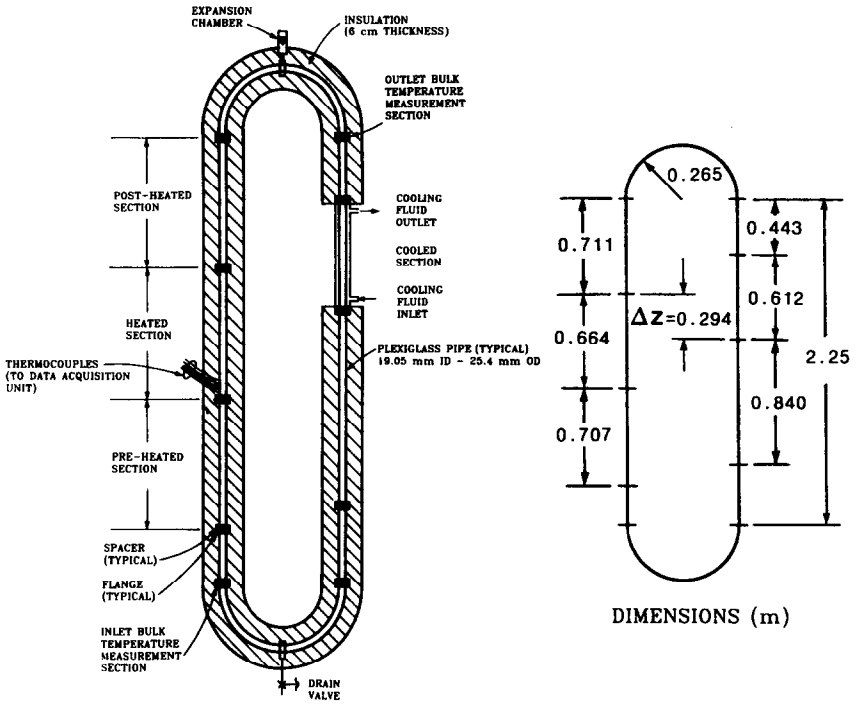

FIG. 3. Schematic of the experimental closed-loop thermosyphon.

sition from one vertical branch to the other with a minimum of form losses. As indicated in Fig. 3, the lengths of the heated and cooled sections are 0.664 and 0.612 m, respectively, and the distance between the centers of these two sections, ΔZ, is 0.294 m. The total circulation length of the closed-loop is 6.2 m. The nominal internal and external diameters of the pipes are 19.05 and 25.4 mm, respectively, except in the pre-heated, heated, and post-heated sections, where a gold-film is attached to the inner surface of the pipe, and the internal diameter is equal to 18 mm. Distilled water is used as the heat transfer fluid, and the loop has a volumetric capacity of about 1.75 l. The loop is open to the atmosphere at the top, via a small expansion chamber, shown in Fig. 3. The whole assembly was insulated with a foamed-plastic pipe insulation (6 cm thick, $k = 0.04$ W m^{-1} °C^{-1}).

As shown in Fig. 3, two bulk temperature measurement sections are used: one, labelled as the inlet bulk temperature measurement section, is located at the left end of the bottom 180° bend; and the other is located at the right end of the upper 180° bend, and labelled as the outlet bulk temperature measurement section. Each of these sections consists of a Plexiglas spacer with five fine (36 gauge) Type-E thermocouples located along the pipe diameter. Each thermocouple measures the temperature of the fluid flowing inside the loop at that particular location. The inlet and outlet bulk temperature measurements, along with the net power input measurement and estimates of heat losses (or gains), were used, as will be shown later, to obtain the average velocity inside the closed-loop.

The cooled section is a double-pipe heat exchanger, designed to provide an essentially constant and uniform wall temperature condition on the inner pipe made of copper. Cooling water, supplied by a 20-l constant temperature bath (Neslab, model RTE-220A), was circulated in the annulus of the cooled section at a flow rate much greater than the flow rate inside the closed-loop, in order to approximate the uniform wall temperature condition on the inner pipe. The inner pipe wall temperature uniformity was continuously monitored using three Type-E thermocouples. Typically, in all runs, the temperatures measured by the three thermocouples were all within 1°C of each other [22].

The pre-heated, heated and post-heated sections are located on the left-hand side of the loop. These three sections are nominally identical. Each section is composed of a Plexiglas pipe, with an internal diameter of 19.05 mm and an external diameter of 25.4 mm, in which a thin semi-transparent gold-film electrical heater has been glued on the inner surface. The resulting internal diameter of these sections is 18 mm.

The heated section was the only one energized during tests, and it was instrumented with thermocouples to measure wall temperatures. The pre-heated and post-heated sections were built to ensure that the internal pipe diameters upstream and downstream of the heated section would be identical to the internal diameter of the heated section. The design and construction details are given elsewhere by Bernier [22]. In the heated section, holes were drilled through the Plexiglas walls to accommodate thermocouples for

wall temperature measurements. It should also be noted that the length of the straight pre-heated section exceeded the Langhaar entrance length estimate [25] in all experiments. Furthermore, axial conduction in the pipe wall and in the fluid was negligible in all cases [22]. Thus the flow could be assumed to be fully developed at the entrance of the heated section.

3.2. *Supporting equipment and instrumentation*

3.2.1. *Temperature measurements.* The chromel–constantan (Type E) thermocouples used in this study were connected to a data acquisition unit (Hewlett-Packard, model 3497A). All thermocouples located in the heated section were individually calibrated against a calibrated quartz thermometer (Hewlett-Packard, model 2804A). Based on these results, the uncertainty in the temperatures measured with the calibrated thermocouples was estimated at $\pm 0.05^{\circ}$C [22].

The ambient temperature was measured using a thermocouple located at the mid-height of the closed-loop. In order to reduce radiation errors, the thermocouple was shielded by inserting it into a 6 mm brass tube.

Final wall temperature measurements in the heated section were taken with 46 thermocouples glued inside the Plexiglas pipe of the heated section. Typically, two thermocouples were positioned 180° apart in each axial measuring cross-section. Uncertainties in the axial and radial positioning of the thermocouples were estimated at ± 0.5 and ± 0.1 mm, respectively.

3.2.2. *Inlet and outlet bulk temperature measurements, $T_{b,in}$ and $T_{b,out}$.* The fluid temperature, density, and velocity profiles are needed to determine the bulk temperature. However, if the temperature is uniform at a given cross-section, then the bulk temperature is simply equal to that temperature, without the need to measure the velocity profile. In this work, the temperature uniformity in the inlet and outlet bulk temperature measurement sections was continuously monitored during all tests, and, typically, all five thermocouples were well within 0.3°C of each other [22]. Thus the inlet and outlet bulk temperatures were assumed equal to the arithmetic average of the five thermocouple measurements.

As shown in Fig. 3, the inlet and outlet bulk temperature measurements were not made immediately at the inlet and outlet of the heated section. This was done for two reasons: first, had the inlet bulk temperature measurement been made at the inlet of the heated section, the immersed thermocouple wires could have affected the inlet velocity profile. Second, because the temperature profile at the outlet of the heated section is not uniform, an outlet bulk temperature measurement at that location would have required, based on the foregoing discussion, a knowledge of the velocity profile. Instead, the outlet temperature measurement was located away from the outlet of the heated section, after the top 180° bend, so as to get a more uniform fluid temperature over the cross-section of the pipe.

3.2.3. *Average velocity measurements.* In this work, the average velocity inside the closed-loop was evaluated using the following relationship:

$$V = \frac{P_w - (Q_x + Q_y + Q_z)}{\rho A C_p (T_{b,out} - T_{b,in})} \tag{21}$$

where Q_x, Q_y and Q_z represent heat losses, from s_1 to s_2, from s_2 to s_3, and from s_3 to s_6, respectively.

Electrical power was provided to the heated section by a DC power supply (Sorensen, model DCR300-3B). Current was measured using a multimeter (Hewlett-Packard, model HP3478A, accuracy = ± 1 mA). Voltage measurements across the heated section were obtained using a separate multimeter (Keithley, model 195A, accuracy = ± 33 mV).

Since one of the main criteria of comparison between the predictions of the proposed 1-D/2-D model and the experimental results is the average velocity, a thorough *in situ* calibration of the average velocity measurements was undertaken, according to the technique recommended by the International Standard Organization [26]. For the calibration tests, the cooled section was removed and replaced by flexible pipes which were connected to a constant head tank and to a bucket. The constant head tank supplied a constant flow rate of water to the loop. This flow rate was determined by measuring the mass of water accumulating in a bucket over a certain time interval measured by a stopwatch. The calibration procedure consisted of comparing, under steady-state conditions, the average velocity obtained using equation (21) with the one given by the stopwatch–bucket method. Details of this calibration are given by Bernier [22], where the uncertainty in the experimentally determined value of V (using equation (21)) is estimated at $\pm 5\%$.

4. RESULTS AND DISCUSSION

4.1. *Preliminary considerations*

The governing equations of the proposed 1-D/2-D model have been non-dimensionalized by Bernier [22]. For the closed-loop thermosyphon shown in Fig. 1, five independent dimensionless parameters emerge from this non-dimensionalization: Gr_m ($= D^3 g\beta q/\nu V_{ref} k_f$), a modified Grashof number; St_m ($= UD/\rho V_{ref} A C_p$), a modified Stanton number; Re_{ref} ($= V_{ref} D/\nu$), a reference Reynolds number; Pr ($= \mu C_p/k_f$), the Prandtl number; ϕ_∞ ($= [T_a - T_w]/[qD/k_f]$), a dimensionless ambient temperature. In these parameters, V_{ref} is the average fluid velocity in the thermosyphon as predicted by case 1 of the traditional 1-D analysis (equation (9)).

In order to test the proposed 1-D/2-D model, it was decided to compare its results against data obtained with the experimental apparatus described in Section 3, for operating conditions which produce strong mixed-convection effects. In all, eight different runs, summarized in Table 1, were considered: for each of these runs, the results of the corresponding numerical

Table 1. Comparison of results obtained with the traditional 1-D model (*cases* (1) and (2)), the proposed 1-D/2-D model, and the experimental apparatus

Run No.	Power input (W)	Heat removed (W)	T_w (°C)	T_a (°C)	Gr_m	St_m	ϕ_∞	Pr	V_{ref} (cm s^{-1})	Experimental data				Proposed 1-D/2-D model				Traditional 1-D model					
																		Case (1)		*Case* (2)			
										V_s (cm s^{-1})	V^*	$T_{b,in}$ (°C)	$T_{b,out}$ (°C)	V_s (cm s^{-1})	V^*	$T_{b,in}$ (°C)	$T_{b,out}$ (°C)	V^*		V^*		$T_{b,in}$ (°C)	$T_{b,out}$ (°C)
1	9.83	12.13	22.0	26.2	1957	0.00088	0.540	6.4	0.3486	0.457	1.311	22.64	24.87	0.465	1.335	22.76	24.92	1.071		1.164		23.32	25.61
2	9.97	10.78	26.9	29.2	2181	0.00078	0.291	5.6	0.3942	0.483	1.225	27.30	29.30	0.473	1.201	27.49	29.51	1.071		1.156		28.36	30.43
3	25.18	28.16	21.3	27.6	3191	0.00054	0.317	6.2	0.5699	0.628	1.102	22.48	26.43	0.626	1.099	22.68	26.62	1.071		1.133		25.53	29.22
4	39.84	43.67	18.9	27.4	3920	0.00044	0.269	6.4	0.6979	0.722	1.112	20.74	26.12	0.704	1.009	20.84	26.35	1.071		1.112		26.02	30.83
5	39.89	45.65	15.7	26.8	3679	0.00047	0.347	6.9	0.6490	0.679	0.973	18.05	23.89	0.690	1.063	17.97	23.71	1.071		1.126		22.81	27.97
6	54.83	60.10	15.8	27.3	4437	0.00039	0.261	6.7	0.7859	0.776	0.987	18.58	25.46	0.756	0.962	18.50	25.55	1.071		1.118		26.06	31.97
7	54.80	62.43	13.2	27.7	4206	0.00041	0.329	7.1	0.7395	0.739	0.999	16.23	23.59	0.746	1.008	16.16	23.45	1.071		1.120		23.34	29.60
8	74.58	81.14	13.3	27.7	5078	0.00034	0.242	6.8	0.8969	0.845	0.942	17.01	25.57	0.814	0.908	16.76	25.65	1.071		1.113		27.70	34.77

simulations revealed the presence of flow reversals in the heated and cooled sections. The power input was varied from 9.83 to 74.58 W (Gr_m = 1957–5078). The average wall temperature in the cooled section, T_w, varied from 13.2 to 26.9°C. As mentioned earlier, the loop was well insulated, with St_m varying from 0.34×10^{-3} to 0.88×10^{-3}, and ϕ_∞ varying from 0.261 to 0.540. In each experimental run, the conditions were considered to be steady when the measured average velocity in the loop did not vary by more than $\pm 1\%$ over a time period equivalent to at least twice the time required for a packet of fluid, travelling at the average velocity, to complete one revolution around the loop.

Form losses, associated with secondary flows in the 180° bends, were accounted for by adding an equivalent length of pipe [22]. Approximate values of the equivalent length of pipe were obtained using the loss coefficients of Blevins [27]. Because of the smoothness of the 180° bends, these form losses amounted to just a few percent of the total frictional losses in the loop. Therefore, they had an essentially negligible impact on the determination of V.

As mentioned earlier, the experimental loop has two slightly different radii: $r_i = 0.009$ m in the preheated, heated, and post-heated sections, and $r_i = 0.0095$ m elsewhere. In the proposed 1-D/2-D model, these two radii were handled by solving the fundamental momentum equation (equation (1)) in the same manner as that described in Section 2, with a proper account of the location of the two radii around the loop. The resulting equation, which is presented in ref. [22], is very similar in form to equation (18). This equation was solved for V_s, the average velocity in the heated section, using the same coupled solution procedure described earlier in Section 2.5. The equation obtained for the traditional 1-D (equation (9)) was also re-derived to account for the two radii of the experimental loop [22].

The 2-D numerical simulations in the extended heated and cooled sections were performed with a non-uniform grid spacing in both the radial and axial directions, with a greater concentration of grid points in regions where steep gradients are expected. Preliminary numerical simulations were undertaken in the extended sections to determine the grid spacings that provided grid-independent results with the proposed 1-D/2-D model. In the axial direction, it was found that in order to get an essentially grid-independent solution, 40 and 30 grid points were necessary in the heated (and cooled) and post-heated (and post-cooled) sections, respectively. Figure 4 presents some of the results of a grid independence check in the radial direction. The conditions used for this grid check are those of experimental run No. 8 (Table 1), which represent the most demanding conditions to simulate. In Fig. 4, the variation of axial velocity with radius at the mid-point in the heated section is plotted for three different radial grid spacing. Based on these and other similar results [22], it was decided to use 10

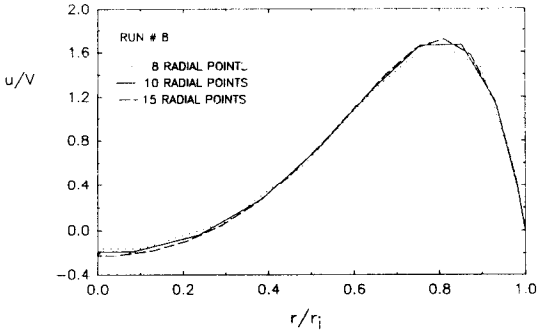

FIG. 4. Some grid independence results for run No. 8: non-dimensional velocity profiles at the mid-point in the heated section, plotted as a function of the non-dimensional radial coordinate for three different grid spacings.

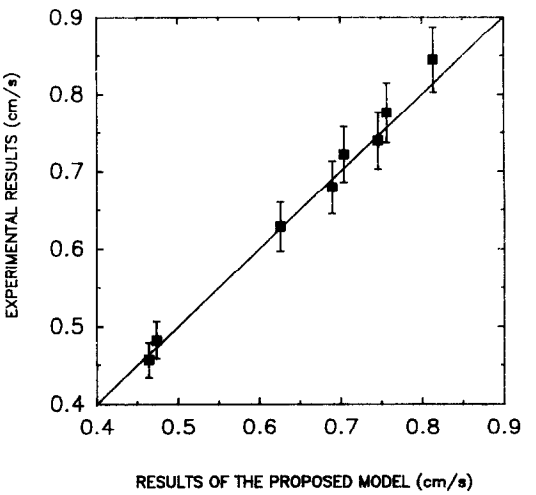

FIG. 5. Average velocity in the heated section of the closed-loop thermosyphon: comparison between experimental data and the results of the proposed 1-D/2-D model.

grid points in the radial direction, as this grid spacing provided an essentially grid-independent solution.

Figure 4 also shows that the distortion, from the inlet parabolic shape, of the velocity profile in the heated section is important. This is because the buoyancy forces become relatively important when compared with the inertia forces (high Gr_q/Re^2) [28]. Therefore, the flow tends to accelerate in the region of the highest temperature (in the vicinity of the wall). To satisfy local mass conservation requirements, the increase in fluid velocity and associated mass flow rate in the vicinity of the wall is fed by fluid drawn from the central region of the pipe. The end result is a steep velocity gradient at the wall, which implies a high Fanning friction factor, and a negative axial velocity (flow reversal) in the center of the pipe.

Suitable lengths of the post-heated and post-cooled sections for both geometries were determined based on preliminary simulations. These post-sections were considered to be long enough when the value of $f\,Re$ at the end of the post-heated sections was within approximately 20% of $f\,Re = 16$. This criterion appears, although no optimization studies were undertaken, to be a reasonable compromise between the accuracy of the model and computational cost. Using this criterion, the lengths of the post-heated and post-cooled sections were the same as the lengths of the heated and cooled sections, 0.664 and 0.612 m, respectively.

4.2. *Average velocity in the heated section*

Figure 5 presents a comparison between the experimentally determined average velocity in the heated section of the closed-loop thermosyphon, V_s, and the corresponding predictions of the proposed 1-D/2-D model. These data are also presented in Table 1, where all the results for a particular run were obtained by assuming constant properties evaluated at the mean loop temperature, as determined by the proposed 1-D/2-D model. It should be noted in this context, that the average velocities were only marginally affected ($<1.5\%$) when calculations were performed with variable properties [22].

The diagonal line in Fig. 5 represents a line of perfect agreement between the results of the proposed model and the experimental measurements. The error bars are the uncertainties in the measured average velocity ($\pm 5\%$). They are based on a calibration of the average velocity measurement procedure, as described earlier. The agreement between the proposed model and the experiments is very good: the line of perfect agreement lies totally within the range of the experimental uncertainty bars. Therefore, the proposed 1-D/2-D model can be considered to be validated over this range of conditions.

Figure 6 presents the results of a comparison between *cases* (1) and (2) of the traditional 1-D model, and the proposed 1-D/2-D model for the eight runs presented in Table 1. Non-dimensional average velocities in the heated section, $V^* = V_s/V_{rel}$, are plotted against Gr_m.

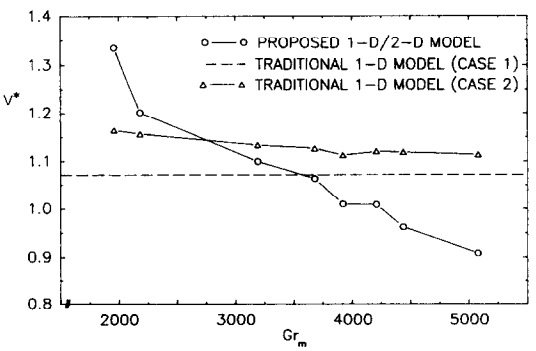

FIG. 6. Variation of V^* as a function of Gr_m: comparison between the traditional and proposed 1-D/2-D models.

As indicated in Fig. 6, for *case* (1) of the traditional 1-D model, V^* is independent of Gr_{in}. It should be noted again that the internal radius of the heated section (and pre- and post-heated sections) is different from that in the other sections of the loop: therefore, $V_s \neq V_{ref}$. It can also be seen that the results for *case* (2) of the traditional 1-D model tend towards those of *case* (1) for large values of Gr_m. This is because as Gr_m increases, V_s increases and X decreases. Thus, the argument of the exponential function in equation (8) decreases, which results in a temperature profile, in the cooled section, which tends towards a linear profile. Since *case* (1) produces a linear temperature variation in the cooled section, it is not surprising to see that the V^* results of *cases* (1) and (2) tend towards the same value as Gr_m increases.

The general trend of the curve for the proposed 1-D/2-D model indicates that V^* decreases as Gr_m increases. For small Gr_m, the results for *cases* (1) and (2) of the traditional 1-D model are lower than the ones predicted by the proposed 1-D/2-D model. Conversely, for high Gr_m, the results for *cases* (1) and (2) are higher than the results of the proposed 1-D/2-D model. These discrepancies between the results of *cases* (1) and (2) of the traditional 1-D analysis and the proposed 1-D/2-D model are mainly due to two factors: (i) the inability of the traditional 1-D models to handle heat losses (or gains) from the insulated portions of the loop; and (ii) the inadequacy of the fully developed flow and heat transfer assumption in traditional 1-D models when strong mixed-convection effects are present in the heated and cooled sections.

The effects of the first of these two factors is shown by looking at the results of runs No. 1 and No. 2 (Table 1), for $Gr_m \approx 2000$. These two runs have approximately the same power input (9.83 and 9.97 W) but because of different wall temperatures in the cooled section and ambient temperatures, the value of ϕ_∞ is almost twice as large for run No. 1 than for run No. 2. This, in turn, influences the amount of heat losses (or gains) from the insulated portions of the loop. Indeed, the amount of heat gain from the insulated portions of the loop is equal to 2.30 and 0.81 W for runs No. 1 and No. 2, respectively. Thus, the amount of heat removed in the cooled section (column 3 in Table 1), which is the power input in the heated section plus the cumulative amount of heat gain around the loop, is equal to 12.13 and 10.78 W for runs No. 1 and No. 2, respectively. This changes the temperature distribution in the loop and the value of V^* [22, 29], as evidenced by the sharp decrease in V^* from run No. 1 to run No. 2 for the proposed 1-D/2-D model. Since the traditional 1-D models do not account for heat losses (or gains), it is not surprising to see differences in the values of V^*, between runs No. 1 and No. 2, obtained with the proposed 1-D/2-D model and *cases* (1) and (2) of the traditional 1-D model.

Heat gains are also present for high values of Gr_m (Table 1), and they are partly responsible for the discrepancy between the values of V^* predicted by the proposed 1-D/2-D and traditional 1-D models. Strong mixed-convection effects also cause this discrepancy. For example, for run No. 8 ($Gr_m = 5078$), Fig. 4 shows that the axial velocity distribution in the heated section is greatly distorted from its fully developed parabolic shape. A similar distortion is also present in the cooled section [22]. Because of these distortions, the value of $f\,Re$ is far from its fully developed value of 16. Indeed, for run No. 8, the value of $f\,Re$ is equal to 78 at the mid-point in the heated section and the average value of $f\,Re$ for the entire loop is 33.1 [22]. Consequently, because of these high frictional losses, the V^* predicted by the proposed 1-D/2-D model is smaller than the ones predicted by the traditional 1-D models. The strong mixed-convection effects in the heated and cooled sections also affect the temperature distribution, $T(s)$, in the loop and the determination of the average velocity [22]. However, the increase in the value of $f\,Re$ is the dominant factor here.

As can be seen in Fig. 6, the curves for *case* (2) of the traditional 1-D model and for the proposed 1-D/2-D model do not vary smoothly as Gr_m increases. This is due to the fact that the thermal properties were evaluated, for each Gr_m, based on the mean loop temperature for that particular run. Since the mean loop temperature varied from test to test, depending mainly on the value of T_w (and to a lesser extent on T_a), the thermal properties varied slightly from one test to the other. For example, runs No. 4 and No. 5 (near $Gr_m \approx 4000$ in Fig. 6) had approximately the same power input to the loop, 39.84 and 39.89 W, respectively, but the wall temperatures in the cooled section were different, 18.85 vs 15.70°C. Consequently, the mean loop temperature and the thermal properties were not the same, which, in turn, influenced the value of V^* as evidenced by the 'dip' in the curve for *case* (2) near $Gr_m \approx 4000$. The same argument can be made to explain the behavior of the curve of the proposed 1-D/2-D model in the vicinity of $Gr_m \approx 4000$.

4.3. *Axial wall temperature variations in the heated section*

The local variations of the wall temperatures in the heated section are presented in Figs. 7(a)–(c) for three different power inputs as a function of the non-dimensional coordinate, z/D. As indicated earlier, the uncertainty in these experimental results was estimated at ± 0.05°C. The uncertainty associated with the positioning of the thermocouples was ± 0.5 mm. Both of these uncertainty values are well within the diameter of the dots presented in Fig. 7. The solid lines plotted in Figs. 7(a)–(c) refer to the local wall temperatures predicted by the proposed 1-D/2-D model and were obtained by assuming constant fluid properties evaluated at T_m.

As can be seen, the agreement between the local predictions of the proposed model and the experimental measurements is quite good at low power

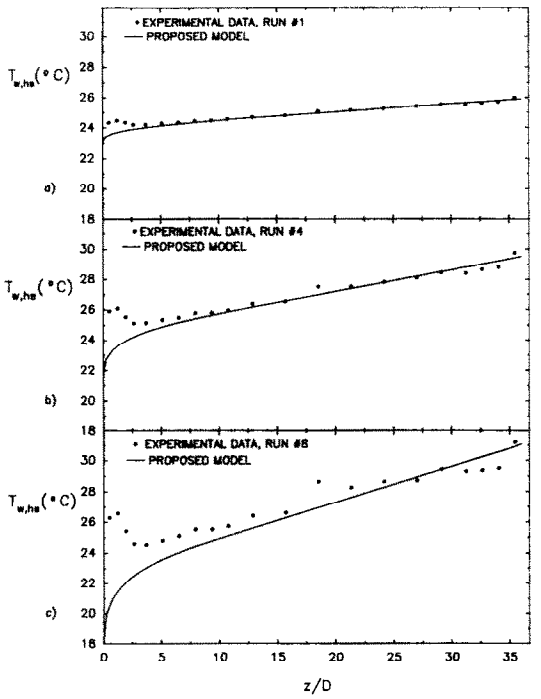

FIG. 7. Axial variation of wall temperatures in the heated section: comparison between experimental data and the results of the proposed 1-D/2-D model.

levels, Figs. 7(a) and (b), but there is a deterioration in the level of agreement at high power, Fig. 7(c). In all three cases, the measured wall temperatures are higher than the numerical predictions in the entrance region of the heated section, at $z/D \approx 0$. As reported by Bernier [22], it is believed that, under the conditions of thermal expansion and contraction experienced by the heated section, the electrical link between the gold-film and the copper electrodes weakened with time, causing a local increase in the value of the electrical resistance at the electrode–film interface. This created a greater-than-average heat flux and higher-than-normal wall temperatures, as seen in Fig. 7, in the vicinity of these locations. There also appears to be a slight defect in the gold-film near $z/D \approx 18$, as shown by the results in Fig. 7(c) [22].

4.4. *Bulk temperatures*

Inlet and outlet bulk temperatures were measured at two locations in the experimental apparatus (Fig. 3). These measurements, along with the corresponding predictions of the proposed 1-D/2-D and the traditional 1-D models, are presented in Table 1. As can be seen, the values of $T_{b,in}$ and $T_{b,out}$ predicted by the proposed 1-D/2-D model are in good agreement with the experimental data; the maximum difference is 0.25°C for run No. 8. This is in contrast with the results of *case* (2) of the traditional 1-D model which do not compare favorably with the experimental data. For example, for run No. 8, there is a 10.7°C difference in the value of $T_{b,in}$ predicted by *case* (2) and the one measured experimentally. This emphasizes, once more, the inability of traditional 1-D models to make accurate predictions in the presence of strong mixed-convection effects and heat losses (or gains).

5. CONCLUDING REMARKS

A new approach to the modeling of closed-loop thermosyphons with vertical heat transfer sections has been proposed. It involves an iterative procedure which couples the local results of 2-D numerical simulations performed in the extended heated and cooled sections with those of a 1-D model. The outputs of the solution include the average velocity in the closed-loop, 2-D velocity and temperature fields in the extended heated and cooled sections, and nodal temperatures around the loop.

In comparisons with results of a complementary experimental study, the proposed 1-D/2-D model successfully predicted the average velocity and bulk temperatures at two locations in the loop, over the range of power inputs studied in this work, from 9.83 to 74.58 W ($Gr_m = 1957$–5078). In addition, the 1-D/2-D model put forward in this work was able to predict fairly well, especially at low power levels, local wall temperature measurements made in the heated section of the closed-loop thermosyphon.

A comparison between the proposed 1-D/2-D and traditional 1-D models indicated that these latter models can be quite inaccurate when strong mixed-convection effects are present in the heated and cooled section of the loop and/or when heat losses (or gains) from the insulated portions of the loop are significant.

Acknowledgements—This research was financially supported by the Natural Sciences and Engineering Research Council of Canada in the form of a Post-graduate Scholarship granted to M. A. Bernier and through individual operating grants awarded to Prof. Baliga.

REFERENCES

1. P. Welander, On the oscillatory instability of a differentially heated fluid loop, *J. Fluid Mech.* **29**, 17–30 (1967).
2. J. S. Glen and J. W. Hilborn, The Canadian slowpoke heating reactor, *Proc. of a Tech. Committee Meeting and Workshop on Nuclear Heat Application*, IAEA, Cracow, Poland, pp. 129–139, 5–9 December (1984).
3. D. Japkise, Advances in thermosyphon technology. In *Advances in Heat Transfer* (Edited by T. F. Irvine and J. P. Hartnett), Vol. 9, pp. 1–111. Academic Press, New York (1973).
4. Y. Zvirin, A review of natural circulation loops in pressurized water reactors and other systems, *Nucl. Engng Des.* **67**, 203–225 (1981).
5. H. Tabor, Some thoughts on water heaters for rural areas, *Sunworld* **8**, 44–46 (1984).
6. A. Mertol, W. Place, T. Webster and R. Greif, Detailed loop model (DLM) analysis of liquid solar thermosiphons with heat exchangers, *Solar Energy* **27**, 367–386 (1981).

7. M. G. Parent, Th. H. Van Der Meer and K. G. T. Hollands, Natural convection heat exchangers in solar water heating systems: theory and experiment, *Solar Energy* **45,** 43–52 (1990).
8. A. Mertol and R. Greif, A review of natural circulation loops. In *Natural Convection Fundamentals and Applications* (Edited by S. Kakaç, W. Aung and R. Viskanta), pp. 1033–1071. Hemisphere, Washington, D.C. (1985).
9. R. Greif, Natural circulation loops, *ASME J. Heat Transfer (50th Anniversary Issue)* **110,** 1243–1258 (1988).
10. A. Mertol, Heat transfer and fluid flow in thermosyphons, Ph.D. thesis, University of California, Berkeley (1980).
11. P. S. Damerell and R. J. Schoenhals, Flow in a toroidal thermosyphon with angular displacement of heated and cooled sections, *ASME J. Heat Transfer* **101,** 672–676 (1979).
12. K. P. Hallinan and R. Viskanta, Heat transfer from a vertical tube bundle under natural circulation conditions, *Int. J. Heat Fluid Flow* **6,** 256–264 (1985).
13. B. J. Huang and R. Zelaya, Heat transfer behavior of a rectangular thermosyphon loop, *ASME J. Heat Transfer* **110,** 487–493 (1988).
14. J. S. Lewis, M. W. Collins and P. H. G. Allen, Flow rate predictions for a thermosyphon loop, *Proc. of the 9th Int. Heat Transfer Conf.*, Jerusalem, Israel, Vol. 2, pp. 549–554 (1990).
15. A. Mertol, R. Greif and Y. Zvirin, Two-dimensional study of heat transfer and fluid flow in a natural convection loop, *ASME J. Heat Transfer* **104,** 508–514 (1982).
16. B. R. Durig and M. A. Shadday, Flow in a rectangular closed-loop thermosyphon with vertical heat transfer passages, ASME paper 86-WA/HT-78 (1986).
17. A. G. Lavine, A three-dimensional analysis of natural convection in a toroidal loop, Ph.D. thesis, University of California, Berkeley (1984).
18. H. F. Creveling, J. F. De Paz, J. Y. Baladi and R. J. Schoenhals, Stability characteristics of a single-phase free convection loop, *J. Fluid Mech.* **67,** 65–84 (1975).
19. C. H. Stern, R. Greif and J. A. C. Humphrey, An experimental study of natural convection in a toroidal loop, *ASME J. Heat Transfer* **110,** 877–884 (1988).
20. P. K. Vijayan and A. W. Date, Experimental and theoretical investigations on the steady-state and transient behaviour of a thermosyphon with throughflow in a figure-of-eight loop, *Int. J. Heat Mass Transfer* **33,** 2479–2488 (1990).
21. B. J. Huang, A combined convection correlation for vertical downward cooling flow in a natural circulation loop, *Int. J. Heat Mass Transfer* **30,** 1544–1546 (1987).
22. M. A. Bernier, Investigation of a closed-loop thermosyphon, Ph.D. thesis, McGill University, Montréal, Canada (1991).
23. S. V. Patankar, *Numerical Heat Transfer and Fluid Flow*. Hemisphere, Washington, D.C. (1980).
24. J. P. Van Doormaal and G. D. Raithby, Enhancements of the SIMPLE method for predicting incompressible fluid flows, *Numer. Heat Transfer* **7,** 147–163 (1984).
25. W. M. Kays and M. E. Crawford, *Convective Heat and Mass Transfer*. McGraw-Hill, New York (1980).
26. International Standard Organization, Mesure de débit des liquides dans les conduites fermées—Méthode par pesée, Norme Internationale ISO 4185-1980(F) (1980).
27. R. D. Blevins, *Applied Fluid Dynamics Handbook*. Van Nostrand Reinhold, Amsterdam (1984).
28. M. A. Bernier and B. R. Baliga, Conjugate conduction and laminar mixed-convection in vertical pipes for upward flow and uniform wall heat flux, *Numer. Heat Transfer—Applications Part A* **21,** 313–332 (1992).
29. M. A., Bernier and B. R. Baliga, Effects of heat losses (or gains) from insulated portions of closed-loop thermosyphons with vertical heat transfer sections, *ASME J. Heat Transfer* (in press).

MODELE 1D/2D ET RESULTATS EXPERIMENTAUX POUR UN THERMOSIPHON A BOUCLE FERMEE AVEC DES SECTIONS VERTICALES DE TRANSFERT THERMIQUE

Résumé—On propose un nouveau modèle 1D/2D pour des thermosiphons à boucle fermée avec des sections verticales de transfert de chaleur. Ce modèle améliore les résultats des modèles traditionnels 1D pour les cas où : (i) les effets de convection mixte sont importants pour les sections chaudes et froides de la boucle ; et (ii) les pertes (ou gains) de chaleur dans les parties isolées sont significatives. Ceci est obtenu en couplant itérativement les résultats locaux des simulations numériques 2D des écoulements de convection mixte dans les sections chaudes et froides, avec une surface 1D. Le modèle est validé en comparant ses résultats avec ceux d'une étude expérimentale complémentaire. Les résultats incluent les prédictions et les mesures de vitesse moyenne dans la boucle, les températures de mélange du fluide. L'accord entre les prédictions du modèle et les résultats expérimentaux se révèle très bon.

EIN-/ZWEI-DIMENSIONALE NUMERISCHE UND EXPERIMENTELLE UNTERSUCHUNG EINES SCHLEIFENFÖRMIGEN THERMOSYPHONS MIT SENKRECHTEN WÄRMEÜBERTRAGUNGSSTRECKEN

Zusammenfassung—In der vorliegenden Arbeit wird ein neues ein-/zwei-dimensionales Modell für einen schleifenförmigen Thermosyphon mit senkrechten Wärmeübertragungsstrecken vorgestellt. Dieses Modell liefert für folgende Fälle bessere Ergebnisse als herkömmliche eindimensionale Modelle : (i) wenn in Heiz- und Kühlzone der Schleife Einflüsse der Mischkonvektion wesentlich sind ; (ii) wenn Wärmeverluste (odergewinne) in den isolierten Teilen der Schleife bedeutsam sind. Dies wird durch eine iterative Kopplung örtlicher Ergebnisse zweidimensionaler numerischer Simulationen der Mischkonvektionsströmung in der Heiz- und der Kühlzone mit einer eindimensionalen Analyse ermittelt. Das vorgestellte ein-/zwei-dimensionale Modell wird durch Vergleich mit entsprechenden Ergebnissen einer experimentellen Untersuchung validiert. Folgende Größen werden vorausberechnet bzw. gemessen : mittlere Geschwindigkeit in der Schleife, örtliche Wandtemperaturen in der Heizzone, Kerntemperaturen des Fluids. Die Übereinstimmung zwischen Berechnung und Messung erweist sich als sehr gut.

ОДНОМЕРНАЯ (ДВУМЕРНАЯ) МОДЕЛЬ И ЭКСПЕРИМЕНТАЛЬНЫЕ РЕЗУЛЬТАТЫ ДЛЯ ТЕРМОСИФОНА С ЗАМКНУТЫМ КОНТУРОМ И ВЕРТИКАЛЬНЫМИ ТЕПЛООБМЕННЫМИ СЕКЦИЯМИ

Аннотация—Предложена новая одномерная (двумерная) модель для термосифонов с замкнутым контуром и вертикальными теплообменными секциями. Данная модель дает более точные результаты, чем традиционные одномерные, в случаях, когда: (i) эффекты смешанной конвекции являются существенными в нагреваемой и охлаждаемой секциях контура и (ii) потери (или приращения) тепла на изолированных участках контура являются значительными. Это достигается посредством итерации при расчете двумерных смешанноконвективных течений в нагреваемой и охлаждаемой секциях с учетом результатов одномерного анализа. Эффективность новой модели проверяется путем сравнения полученных на ее основе результатов с данными экспериментального исследования для средней скорости в контуре, локальных температур в нагреваемой секции контура и среднемассовых температур жидкости. Показано, что расчеты по предложенной модели очень хорошо согласуются с эксперимеитальными данными.